

# **Magnetic Signatures of the Interaction Between Europa and Jupiter's Magnetosphere During the Juno Flyby**

**Peter Addison<sup>1,a</sup>, C. Michael Haynes<sup>1,a</sup>, Aaron M. Stahl<sup>1,2,a</sup>, Lucas Liuzzo<sup>3,a</sup>, and Sven Simon<sup>1,2,a</sup>**

<sup>1</sup>School of Earth and Atmospheric Sciences, Georgia Institute of Technology, 311 Ferst Drive, Atlanta, GA 30332-0340, USA

<sup>2</sup>School of Physics, Georgia Institute of Technology, 837 State Street, Atlanta, GA 30332-0430, USA

<sup>3</sup>Space Sciences Laboratory, University of California, Berkeley, 7 Gauss Way, Berkeley, CA 94720, USA

<sup>a</sup>All five authors contributed equally to this study.

## **Key Points:**

- By applying a hybrid model (kinetic ions, fluid electrons), we study Europa's interaction with Jupiter's magnetosphere during the Juno flyby
- A dawn-dusk asymmetry in Europa's atmosphere can reproduce the large-scale structure of the draping signatures seen by the Juno magnetometer
- The spacecraft encountered the center of Europa's southern Alfvén wing during ingress and the periphery of the northern wing during egress

---

Corresponding author: Sven Simon, [sven.simon@eas.gatech.edu](mailto:sven.simon@eas.gatech.edu)

**Abstract**

Based on a hybrid model of Europa's magnetospheric interaction, we provide context for the magnetic field perturbations observed by the Juno spacecraft during its only close flyby of the moon in September 2022. By systematically varying the incident flow conditions and the density profile of Europa's atmosphere, we demonstrate that the observed, large-scale signatures of magnetic field draping are consistent with a dawn-dusk asymmetry in the moon's neutral envelope. During the flyby, such an asymmetry would have enhanced the magnetic perturbations in Europa's anti-Jovian hemisphere, explaining why the spacecraft already detected strong field line draping while still several moon radii away. Conversely, a reduced neutral density in the sub-Jovian hemisphere can explain why the perturbations in the flow-aligned field component remained nearly constant as Juno approached Europa. While a dawn-dusk asymmetry in Europa's atmosphere has been predicted by theoretical work, our results provide the first in-situ hints of its presence.

**Plain Language Summary**

Located within Jupiter's magnetosphere, the small Galilean moon Europa is continuously exposed to a flow of magnetized plasma, traveling at a relative velocity of about 100 km/s. The deflection of this plasma around Europa generates perturbations to Jupiter's magnetic field, as observed for the first time in two decades during the flyby of the Juno spacecraft in 2022. The magnitude and extension of these magnetic perturbations are largely determined by the shape of Europa's atmosphere and ionosphere which represent obstacles to the incident magnetospheric plasma. To provide three-dimensional context for the structure of Europa's magnetic environment at the time of the Juno flyby, we have applied a computer simulation to study the moon's interaction with the plasma flow. Comparison between modeled and observed magnetic fields suggests that, at the time when Juno collected these data, Europa's atmosphere may have been denser in the anti-Jovian than in the Jupiter-facing hemisphere. Theoretical predictions suggest such an asymmetry to be present in Europa's neutral envelope, partially generated by centrifugal and Coriolis forces acting on the gas molecules during the moon's rotation around Jupiter. Our study reveals first hints from a spacecraft flyby that such a hemispheric asymmetry may indeed exist in Europa's atmosphere.

## 47 1 Introduction

48 Europa, the smallest of Jupiter's Galilean moons (radius  $R_E = 1,560.8\text{ km}$ ), has  
49 been visited by the Galileo spacecraft during eleven close flybys between 1996 and 2000.  
50 Magnetic field observations from these encounters revealed the presence of a time-varying,  
51 internal dipole moment at Europa that stems from currents induced within a conduct-  
52 ing subsurface ocean (Kivelson et al., 2000; Zimmer et al., 2000; Schilling et al., 2007).  
53 Galileo also detected a strong interaction between Europa and the incident magnetospheric  
54 plasma: the moon's oxygen-rich atmosphere (e.g., Plainaki et al. (2018)) is partially ion-  
55 ized by electron impacts (Saur et al., 1998), and newly generated ions are incorporated  
56 into the magnetospheric flow, draining momentum from it and causing its deflection around  
57 the obstacle (Kivelson et al., 2009). The induced dipole also contributes to the modi-  
58 fication of the flow pattern and magnetospheric field near Europa (e.g., Neubauer (1999);  
59 Volwerk et al. (2007)). The impinging magnetospheric field lines pile up at Europa's ram-  
60 side, forming a draping pattern and connecting to a system of Alfvén wings at larger dis-  
61 tances to the moon (e.g., Neubauer (1980, 1998)).

62 To provide three-dimensional context for magnetic field data collected along the  
63 Galileo flyby trajectories, a broad pallet of models has been applied to study Europa's  
64 interaction with the Jovian magnetosphere (e.g., Jia et al. (2018); Arnold et al. (2019);  
65 Harris et al. (2021)). However, currently there is no comprehensive description available  
66 that captures the structure of Europa's atmosphere for any given combination of the moon's  
67 orbital position (defined by the Jovian Local Time) and its distance to the center of Jupiter's  
68 magnetospheric plasma sheet (defined by the System III longitude). Therefore, any such  
69 plasma interaction model inherently needs to make assumptions on potential asymme-  
70 tries present in Europa's neutral gas envelope. For instance, the magnetohydrodynamic  
71 (MHD) model of Blöcker et al. (2016) treated the moon's global O<sub>2</sub> atmosphere as spher-  
72 ically symmetric, and this symmetry is broken only by localized plumes of water vapor  
73 at various positions across the surface. The MHD models of Rubin et al. (2015), Jia et  
74 al. (2018), and Harris et al. (2021, 2022) as well as studies with the AIKEF hybrid model  
75 (e.g., Arnold et al. (2019); Addison et al. (2021)) assumed a ram-wake asymmetry to be  
76 present in Europa's O<sub>2</sub> envelope, i.e., the neutral density in these models peaks at the  
77 moon's ramside apex and is reduced in the wakeside hemisphere. This assumption is based  
78 on the notion that surface sputtering by energetic ions (a major contributor to Europa's  
79 atmosphere) is largely concentrated around the moon's ramside apex (Cassidy et al., 2013).

80 The presence of enhanced ion sputtering rates near the ramside apex was recently put  
81 into question by Addison et al. (2021, 2022) who calculated the trajectories of the in-  
82 cident energetic ions in a realistically draped electromagnetic environment. In their re-  
83 cent MHD modeling study, Cervantes and Saur (2022) again treated Europa's O<sub>2</sub> atmo-  
84 sphere as spherically symmetric. These authors also included a "bulge" of enhanced H<sub>2</sub>O  
85 density around the moon's dayside (or ramside) apex, consistent with observations by  
86 the Hubble Space Telescope (Roth, 2021).

87 Oza et al. (2019) developed a Monte Carlo model of O<sub>2</sub> dynamics in Europa's at-  
88 mosphere, taking into account the moon's motion around Jupiter along its 85-hour or-  
89 bit and the associated, tidally-locked rotation around its polar axis. Under the assump-  
90 tion that O<sub>2</sub> is mainly generated near Europa's dayside apex, Oza et al. (2019) demon-  
91 strated the presence of a dawn-dusk asymmetry in the neutral gas density: an atmospheric  
92 "bulge" is formed in Europa's dusk hemisphere, while a corresponding reduction in col-  
93 umn density was identified in the dawn hemisphere. Depending on surface location, the  
94 model of Oza et al. (2019) suggests O<sub>2</sub> column densities in the range of  $(7.4 - 8.1) \cdot 10^{17} \text{ m}^{-2}$ .  
95 The dawn-dusk asymmetry of Europa's atmosphere proposed by these authors has not  
96 yet been included in any model of the moon's plasma interaction.

97 On 29 September 2022, the Juno spacecraft carried out its only close flyby of Eu-  
98 ropa, reaching a closest approach altitude of 354.5 km ( $0.23R_E$ ) at 09:36:29 UTC. Fig-  
99 ure 1 displays the trajectory of this flyby in the Cartesian EPhiO coordinate system. The  
100 origin of this system coincides with the center of Europa. Its (+X) axis is aligned with  
101 the direction of corotation, and the (+Y) axis points toward Jupiter. The (+Z) axis com-  
102 pletes the right-handed system, pointing northward. Juno approached Europa from its  
103 anti-Jovian side while traveling northward and toward upstream. However, the space-  
104 craft remained downstream of the moon during most of the flyby. The encounter occurred  
105 at a Jovian Local Time of 18:40, i.e., the direction of the incident magnetospheric plasma  
106 was nearly aligned with the Sun-Europa line (see Figure 1(b) in Liuzzo et al. (2015)).  
107 In other words, Europa's dusk terminator was located in the anti-Jovian half space ( $Y <$   
108 0), approximately 90° in longitude eastward of the subsolar point. For this reason, Eu-  
109 ropa's location during the Juno flyby facilitates the search for any dawn-dusk asymme-  
110 tries in the plasma interaction region which, in turn, may provide hints of similar hemi-  
111 spheric dichotomies in the moon's neutral envelope.

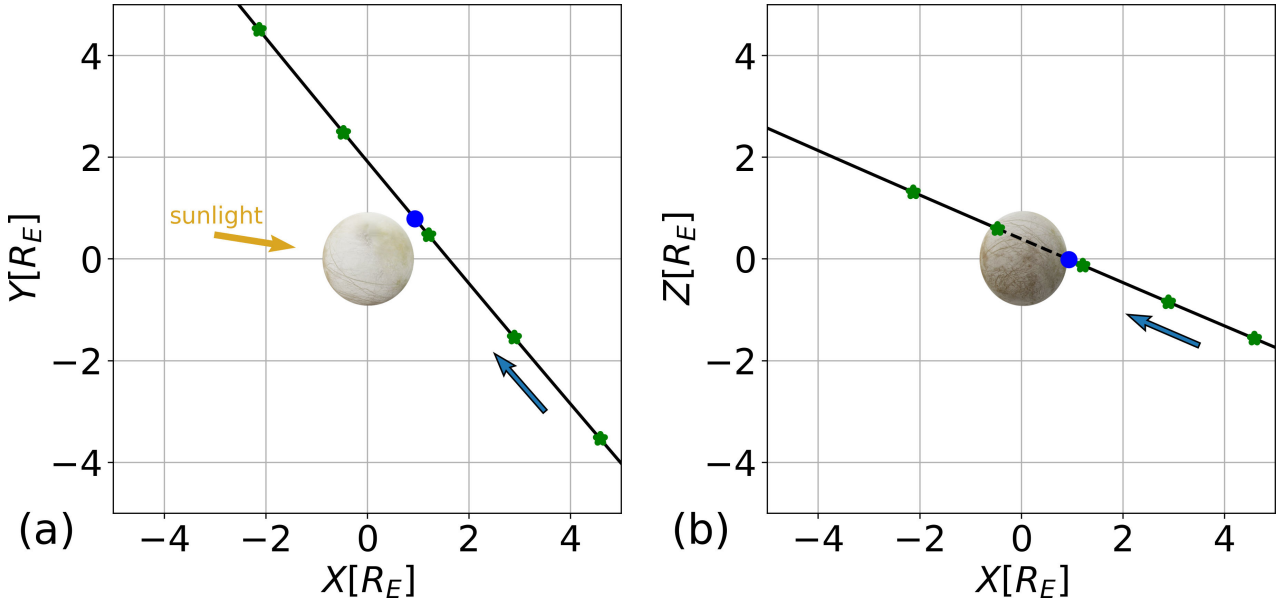


**Figure 1.** Trajectory of the Juno spacecraft during its close flyby of Europa on 29 September 2022. The panels display the projections of the trajectory onto the (a)  $Z = 0$  and (b)  $Y = 0$  planes of the EPhiO system. The blue circle represents the position of Juno’s closest approach at 09:36:29 UTC. The green asterisks along the trajectory are 3 minutes apart, starting at 09:30:00 UTC. During the dashed portion of the trajectory in panel (b), Juno was located “behind” Europa in the  $Y > 0$  half space. The blue arrow denotes Juno’s direction of travel. The orange arrow in panel (a) represents the direction of the incident solar radiation.

In this letter, we analyze the time series recorded by Juno’s magnetometer (Connerney et al., 2017) during the Europa flyby. By applying the AIKEF hybrid model (Müller et al., 2011), we demonstrate that a dawn-dusk asymmetry in the moon’s atmosphere provides a possible explanation for the magnetic perturbations observed along the Juno trajectory.

## 2 Application of the AIKEF Hybrid Model to Europa

The AIKEF model treats ions as individual macroparticles, whereas electrons form a massless, charge-neutralizing fluid. The model has an extensive history of applications to Europa’s plasma interaction (Breer et al., 2019; Arnold et al., 2019; Arnold, Liuzzo, & Simon, 2020; Arnold, Simon, & Liuzzo, 2020; Addison et al., 2021, 2022; Addison, Liuzzo, & Simon, 2023; Haynes et al., 2023). To study Europa’s environment during the Juno flyby, we carried out over 60 model runs, systematically varying the incident mag-

netospheric flow conditions and the structure of the moon's atmosphere. This letter discusses results from six of these setups (see Table 1) which were found to be most instructive for the interpretation of Juno magnetometer observations. These six runs assume the ion population of the impinging thermal plasma to consist of a singly charged species with mass  $m_0 = 18.5$  amu (analogous to, e.g., Addison et al. (2021, 2022)) and number density  $n_0 = 100 \text{ cm}^{-3}$ . This value is (approximately) the average between the densities obtained from the empirical models of Bagenal and Delamere (2011) and Roth et al. (2014) for Europa's system III longitude during the flyby ( $\lambda_{III} = 136^\circ$ ). At the time of this writing, ambient plasma moments from the Juno flyby were not yet available in the peer-reviewed literature.

The bulk velocity of the impinging flow is set to  $|\underline{u}_0| = 87 \text{ km/s}$  (setups #1 and #2) or  $|\underline{u}_0| = 100 \text{ km/s}$  (setups #3–#6), which is within the range of velocity magnitudes deduced from Galileo observations (Bagenal & Dols, 2020). In setups #1, #4, and #5, the upstream flow travels along the (+X) direction, while setups #2, #3, and #6 take into account the small radial flow component observed near Europa's orbital distance (Bagenal et al., 2016): in these two configurations, the flow vector  $\underline{u}_0 = u_0 (\cos \phi, \sin \phi, 0)$  is inclined towards Jupiter by  $\phi = 15^\circ$ . This tilt may be caused by radial plasma transport in the Jovian magnetosphere and the angle is within the range covered by the error bars in Figure 5 of Bagenal et al. (2016). The uniform background magnetic field  $\underline{B}_0$  is the same in all six setups and was obtained by interpolating the magnetospheric field observed before entering and after exiting Europa's interaction region (see section 3) to the point of Juno's closest approach. Taking into account equation (2) from Addison et al. (2021), the vector  $\underline{B}_0$  also determines the moon's induced magnetic moment  $\underline{M}_{\text{ind}}$  at the time of the flyby. We use a cuboid-shaped domain with extensions of  $-8R_E \leq X \leq 22R_E$ ,  $-10R_E \leq Y \leq 10R_E$ ,  $-30R_E \leq Z \leq 30R_E$ .

Model setup	#1	#2	#3	#4	#5	#6
$n_0$ [cm $^{-3}$ ]	100	100	100	100	100	100
$u_0$ [km/s]	87	87	100	100	100	100
$\phi$ [ $^{\circ}$ ]	0	15	15	0	0	15
$B_0$ [nT]	(77.2, -120.2, -422.0)	(77.2, -120.2, -422.0)	(77.2, -120.2, -422.0)	(77.2, -120.2, -422.0)	(77.2, -120.2, -422.0)	(77.2, -120.2, -422.0)
$ B_0 $ [nT]	445.5	445.5	445.5	445.5	445.5	445.5
$M_{\text{ind}}$ [ $\cdot 10^{18}$ J/T]	(-1.4, 2.0, 0)	(-1.4, 2.0, 0)	(-1.4, 2.0, 0)	(-1.4, 2.0, 0)	(-1.4, 2.0, 0)	(-1.4, 2.0, 0)
$\beta_i$	$4.6 \cdot 10^{-2}$	$4.6 \cdot 10^{-2}$	$4.6 \cdot 10^{-2}$	$4.6 \cdot 10^{-2}$	$4.6 \cdot 10^{-2}$	$4.6 \cdot 10^{-2}$
$\beta_e$	$4.6 \cdot 10^{-2}$	$4.6 \cdot 10^{-2}$	$4.6 \cdot 10^{-2}$	$4.6 \cdot 10^{-2}$	$4.6 \cdot 10^{-2}$	$4.6 \cdot 10^{-2}$
$ v_{A,0} $ [km/s]	225.9	225.9	225.9	225.9	225.9	225.9
$M_A$	0.39	0.39	0.44	0.44	0.44	0.44
$M_S$	1.9	1.9	2.20	2.20	2.20	2.20
$M_{MS}$	0.38	0.38	0.43	0.43	0.43	0.43
$n_0$ [m $^{-3}$ ]	$5 \cdot 10^{13}$	$5 \cdot 10^{13}$	$5 \cdot 10^{13}$	$5 \cdot 10^{13}$	$5 \cdot 10^{13}$	$5 \cdot 10^{13}$
$H$ [km]	100	100	100	100	100	100
$\lambda$	5	5	5	—	—	5
$A$	—	—	—	10	0	—
Bulge location	anti-Jovian ( $20^{\circ}$ N)	anti-Jovian ( $20^{\circ}$ N)	anti-Jovian ( $20^{\circ}$ N)	ramside	—	anti-Jovian

**Table 1.** AIKEF model parameters. Values of the plasma beta  $\beta_s = \frac{2\mu_0 n_0 k_B T_s}{B_0^2}$  are computed for magnetospheric ions (index  $s = i$ ) and electrons ( $s = e$ ) separately, using temperatures  $T_s$  from Kivelson et al. (2004). The magnitude of the Alfvén velocity  $v_{A,0} = \frac{B_0}{\sqrt{\mu_0 n_0 m_0}}$  as well as the Alfvénic ( $M_A$ ), sonic ( $M_S$ ), and magnetosonic ( $M_{MS}$ ) Mach numbers are also given.

149 A critical input parameter for our model is the shape of Europa's atmosphere, which  
 150 is partially ionized by electron impacts to form the moon's ionosphere (see, e.g., Arnold  
 151 et al. (2019) for details). Unlike preceding studies with AIKEF (e.g., Addison et al. (2021,  
 152 2022)), setups #1–#3 and #6 no longer include an enhancement in the neutral density  
 153 near Europa's ramside apex and an associated decrease in density around the wakeside  
 154 apex. Instead, we describe the neutral profile  $n_n$  with the expression

$$155 \quad n_n(h, \psi, \lambda) = \begin{cases} n_0 \left[ \cos\left(\frac{\psi}{2}\right) \right]^\lambda \exp\left(\frac{R_E - r}{H}\right) & : \quad \psi \leq 170^\circ \\ n_0 \left[ \cos\left(\frac{170^\circ}{2}\right) \right]^\lambda \exp\left(\frac{R_E - r}{H}\right) & : \quad \psi > 170^\circ \end{cases}, \quad (1)$$

156 where  $r = \sqrt{X^2 + Y^2 + Z^2}$  is the distance to the moon's center and  $H$  is the atmospheric  
 157 scale height. The parameter  $\psi$  denotes the angle between the vector  $\underline{r} = (X, Y, Z)$  and  
 158 a fixed radial unit vector  $\underline{e}$ , pointing from the center of Europa toward a point on the  
 159 moon's surface. The profile defined by equation (1) is axially symmetric around the di-  
 160 rection of  $\underline{e}$ , producing a bulge in number density at  $\psi = 0^\circ$  and a minimum for  $\psi \geq$   
 161  $170^\circ$ . The exponent  $\lambda$  in equation (1) is used to define the "steepness" of the decrease  
 162 in atmospheric density with growing angular distance  $\psi$  from the bulge. A slightly mod-  
 163 ified form of equation (1) was used by Liuzzo et al. (2015) to emulate asymmetries in  
 164 Callisto's neutral envelope.

165 In our setup #6, the location of the atmospheric bulge is defined by  $\underline{e} = (0, -1, 0)$ ,  
 166 i.e., it coincides with the moon's anti-Jovian apex. The Juno flyby occurred around 18:40  
 167 Jovian Local Time; i.e., Europa's duskside apex was displaced by about  $10^\circ$  in longitude  
 168 away from the  $X = 0$  plane and toward the solar apex. However, Figure 4 of Oza et  
 169 al. (2019) shows that their atmospheric density maximum does not occur precisely along  
 170 the semi-meridian at dusk, but is slightly displaced toward the nightside by  $10^\circ - 15^\circ$   
 171 in longitude. These two longitudinal displacements (one toward the dayside, the other  
 172 toward the nightside apex) approximately compensate each other. For our study of the  
 173 Juno flyby, we therefore center the atmospheric bulge around Europa's anti-Jovian apex.

174 Addison et al. (2021) demonstrated that a non-zero  $B_{0,X}$  component of the mag-  
 175 netospheric background field breaks the symmetry of energetic ion precipitation onto the  
 176 moon's surface between its northern and southern hemispheres. The "Case (1)" scenario  
 177 studied by these authors includes a *negative*  $B_{0,X}$  component, and it was revealed that  
 178 this tilt of  $\underline{B}_0$  toward upstream leads to slightly elevated influx of magnetospheric ions  
 179 onto Europa's *southern* hemisphere. Conversely, the *positive*  $B_{0,X}$  component observed

during the Juno flyby (see Table 1) corresponds to enhanced magnetospheric ion precipitation onto Europa's *northern* hemisphere. For this reason, we also explored several configurations with the atmospheric density bulge located along the moon's anti-Jovian semi-meridian, but slightly displaced toward the north: in our setups #1–#3, the location of the atmospheric density peak is defined by  $\underline{e} = (0, -\cos 20^\circ, +\sin 20^\circ)$ , i.e., it is rotated northward by  $20^\circ$  within the  $X = 0$  plane. We emphasize that Addison et al. (2021) did *not* provide a conversion of their modeled ion influx patterns into actual atmospheric density profiles. In this sense, scenarios #1–#3 assume that the north-south asymmetry seen by Addison et al. (2021) in ion precipitation patterns likewise maps into the resulting atmospheric density profile. However, this assumption is currently heuristic in nature and does not follow from rigorous quantitative modeling of Europa's neutral envelope. For all setups discussed here, the values of the atmospheric scale height and the "steepness parameter" have been set to  $H = 100$  km (see, e.g., Addison et al. (2021, 2022); Haynes et al. (2023)) and  $\lambda = 5$ , respectively. Neither parameter was found to have significant influence on the conclusions drawn.

In addition, we have carried out simulations to demonstrate that the atmospheric profiles used in earlier modeling studies are *not* suitable to explain the magnetic signatures observed by Juno. Setup #4 includes a ram-wake asymmetry in the neutral density, using equation (1) from Arnold et al. (2019) and adopting their value of  $A = 10$  for the "asymmetry parameter": the density at Europa's ramside apex then exceeds that at the wakeside apex by a factor of  $A + 1 = 11$ . In setup #5, Europa's neutral envelope is treated as spherically symmetric (analogous to, e.g., Blöcker et al. (2016)), i.e.,  $A$  is set to zero. In all six model setups, Europa's atmosphere is assumed to consist of O<sub>2</sub> only, i.e., we include neither transient plumes of water vapor (Jia et al., 2018; Arnold et al., 2019) nor a bulge of H<sub>2</sub>O molecules around the subsolar or dayside apex (Roth, 2021). Each of these additional atmospheric components was found to generate only very localized perturbations to the magnetic field on length scales much smaller than the extension of the signatures observed by Juno (e.g., Cervantes and Saur (2022); Haynes et al. (2023)). The surface density  $n_0$  in all six setups is chosen such that the column density  $n_0H$  is of the same order ( $\approx 10^{18}$  m<sup>-2</sup>) as derived from remote observations (see, e.g., Addison et al. (2021) for details) and proposed by Oza et al. (2019).

211 **3 Juno Magnetometer Observations and Model Results**

212 In Figure 2 we display Juno magnetic field observations from the Europa flyby as  
 213 well as the synthetic time series from the six AIKEF runs. We also show (in plot (b))  
 214 the magnetic signature obtained by taking the sum of  $\underline{B}_0$  and the induced field from Eu-  
 215 ropa's subsurface ocean. This setup assumes the moon's environment to be devoid of any  
 216 plasma currents. Juno's closest approach to Europa approximately coincided with the  
 217 spacecraft's passage through the  $Z = 0$  plane as it traveled from southern to northern  
 218 latitudes. The geometry of Europa's plasma interaction during this flyby is somewhat  
 219 tricky to capture, since  $\underline{B}_0$  possesses three non-vanishing components. This implies that,  
 220 e.g., none of the three planes of the EPhiO system represents a symmetry plane between  
 221 the moon's northern (−) and southern (+) Alfvén wing characteristics  $\underline{\mathcal{Z}}_{\pm} = \underline{u}_0 \pm \underline{v}_{A,0}$   
 222 (Neubauer, 1980). Besides, while Europa's induced dipole moment is still contained within  
 223 the  $Z = 0$  plane, it is inclined by  $33^\circ$  against the  $Y$  axis.

224 As shown in Figure 2, the observed  $B_X$  component exhibits a broad enhancement,  
 225 commencing in Europa's southern hemisphere around 09:34 UTC and reaching up to  $Z =$   
 226  $+0.6R_E$  into the northern hemisphere (until 09:39 UTC). The occurrence of positive per-  
 227 turbations  $\delta B_X$  (where  $\delta B_i = B_i - B_{0,i}$  for  $i = X, Y, Z$ ) on *both* sides of Europa's  
 228 equatorial plane is not unexpected: due to the tilt of  $\underline{B}_0$  toward downstream ( $B_{0,X} >$   
 229 0, see Table 1), the Alfvén characteristics are rotated counter-clockwise around the ( $+Y$ )  
 230 axis, allowing the southern wing tube (where  $\delta B_X > 0$ ) to penetrate into the north-  
 231 ern half space (e.g., Simon and Motschmann (2009)). Likewise, the northern wing is ro-  
 232 tated away from Juno's trajectory, causing the spacecraft to entirely miss the region of  
 233  $\delta B_X < 0$  associated with  $\underline{\mathcal{Z}}_-$ . Europa's induced dipole alone also generates perturba-  
 234 tions  $\delta B_X > 0$  above the  $Z = 0$  plane (red in Figure 2(b)). In setups that include the  
 235 atmospheric bulge in Europa's anti-Jovian hemisphere (#1–#3 and #6), this  $B_X$  en-  
 236 hancement is further amplified by the plasma interaction.

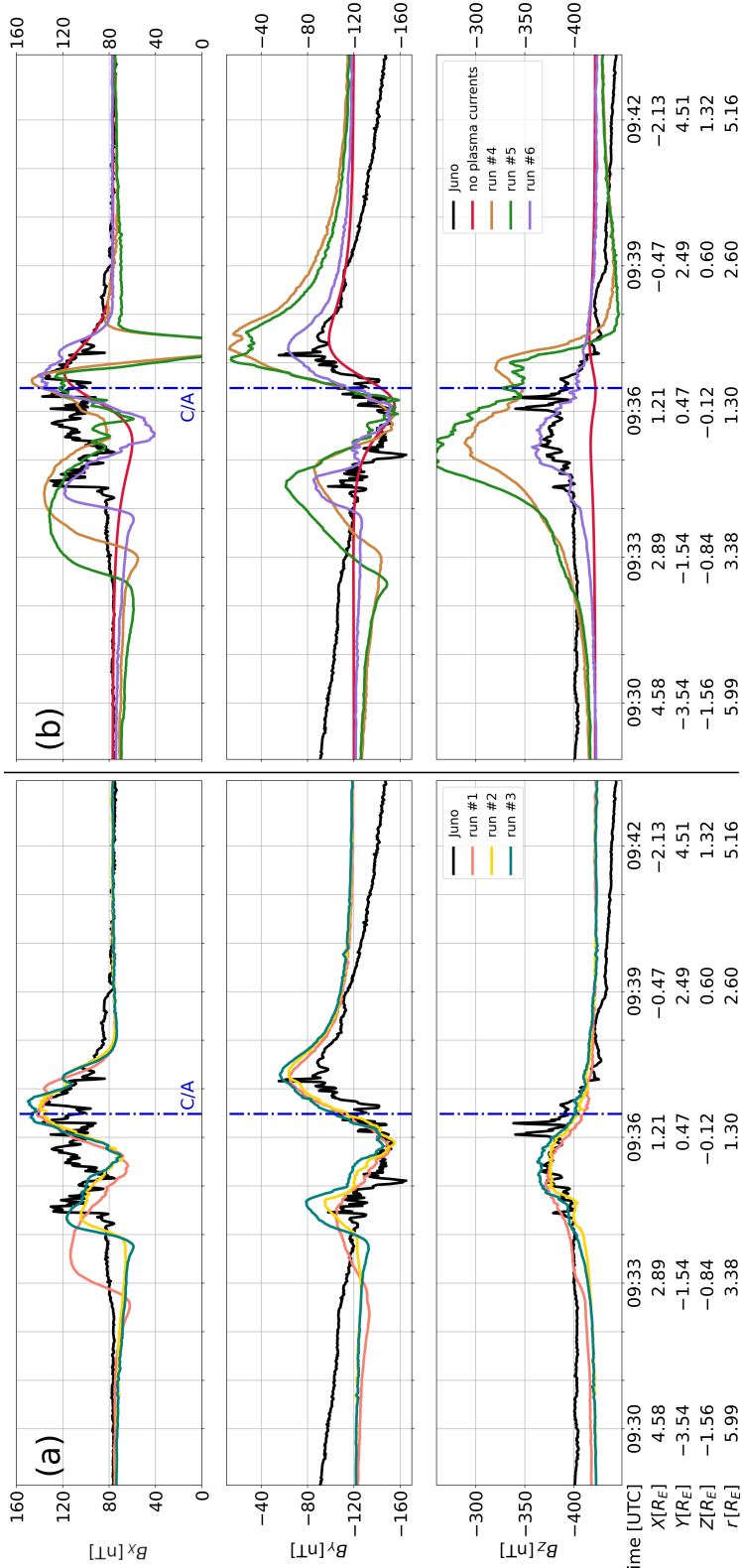


**Figure 2.** Magnetic field  $\underline{B} = (B_x, B_y, B_z)$  near Europa in EPhiO coordinates: model results versus Juno data. The figure displays time series of the observed magnetic field components (black) as well as output from AIKEF runs (a) #1–#3 and (b) #4–#6. Plot (b) also shows the magnetic field obtained from a mere superposition of  $\underline{B}_0$  and Europa's induced dipole (red). The dash-dotted blue line (labeled C/A) denotes the position of Juno's closest approach.

While the  $B_X$  perturbations seen by Juno (black) remained positive throughout the encounter, the strength  $\delta B_X$  of this enhancement changed non-monotonically with time, achieving a broad local minimum in Europa's southern hemisphere around 09:35 UTC. The subsequent  $B_X$  enhancement is "interrupted" by several smaller dips, but these are way less prominent than the feature observed around 09:35. The large-scale shape of the modeled  $B_X$  in setups #1–#3 ("enhancement-dip-enhancement") is similar to the observed signature. However, the locations of the modeled, large-scale  $B_X$  features do not precisely coincide with observations. In these three runs, the central dip is displaced slightly toward upstream: around 09:35:30, AIKEF output still displays the dip while observations show that Juno had already entered the outbound enhancement. These deviations may stem from uncertainties in the atmosphere parameters. The smaller dips imposed on the outbound enhancement are likely caused by fine structures in Europa's ionosphere which the model is not designed to resolve. In setup #1 (which uses  $\phi = 0^\circ$ ), the onset of the modeled  $B_X$  increase occurs about 90 seconds earlier than observed, corresponding to a distance of  $1.3R_E$  traveled along Juno's trajectory. However, setups #2 and #3 almost precisely match the observed location and width of the  $B_X$  enhancement. The slight tilt of  $\underline{u}_0$  toward Jupiter in the latter two setups rotates the Alfvén characteristics into the Jupiter-facing half space. Juno approached Europa from the anti-Jovian side; this implies that in setups #2 and #3 the spacecraft would enter the region of draped field lines later than in setup #1.

Setup #6 (see Figure 2(b)) includes less "fine-tuning" than configurations #2–#3: the atmospheric bulge coincides precisely with Europa's anti-Jovian apex. Nevertheless, the model still matches both the locations and the magnitudes of the two spikes associated with the asymmetric  $B_X$  signature. However, setup #6 overestimates the reduction near the inbound edge of the  $B_X$  feature, with the modeled  $\delta B_X$  clearly turning negative. This run still emphasizes the "robustness" of our conclusions, illustrating that the notion of a dawn-dusk asymmetry in Europa's atmosphere during the Juno flyby can qualitatively explain the shape of the observed  $B_X$  perturbations over a broad range of upstream and atmospheric parameters.

Setups #4 and #5 do not include an atmospheric bulge in the anti-Jovian hemisphere. The magnetic signatures obtained from these runs reveal significant qualitative differences to Juno observations. First, the onset of the inbound  $B_X$  enhancement occurs earlier than detected. Analogous to our discussion of setups #1–#3, this displace-

ment may again be reduced by including a small component of  $\underline{u}_0$  along ( $+Y$ ). Second, and more importantly, runs #4 and #5 both reveal a region of *negative*  $B_X$  in the outbound segment of the flyby, corresponding to a passage through the center of Europa's northern Alfvén wing tube in the  $Z > 0$  half space. Additional simulations suggested that this  $B_X < 0$  feature cannot be eliminated by tilting the upstream flow vector within the observational bounds from Bagenal et al. (2016). The only way we found to prevent Juno's trajectory from intersecting the  $B_X < 0$  region is a localized reduction of the atmospheric column density near Europa's sub-Jovian apex by several orders of magnitude, as realized by equation (1). Using such a low column density ( $\approx 2.5 \cdot 10^{13} \text{ m}^{-2}$ ) *uniformly* across Europa's entire neutral envelope would be inconsistent with magnetometer observations: in this case, the modeled  $B_X$  would be very similar to the "superposition case" (red) that does not include plasma effects. Hence, the observed  $B_X$  perturbations support the notion of Europa's atmosphere at the time of the flyby having been more dense in the anti-Jovian than in the sub-Jovian hemisphere. Such an asymmetric configuration can explain why Juno encountered a strong increase in  $B_X$  while traveling through the anti-Jovian half space and still several  $R_E$  downstream of the moon: the locally enhanced atmospheric density causes the draping to be stronger for  $Y < 0$ . Besides, this atmosphere model can explain why the  $B_X$  enhancement observed close to Europa for  $Y > 0$  is comparable in strength to the inbound feature seen farther downstream: the reduced atmospheric density in the  $Y > 0$  half space locally weakens the plasma interaction; i.e., despite the proximity to Europa the draping signature is not amplified.

The shape of the  $\delta B_Y < 0$  perturbation observed shortly before closest approach can already be matched by the superposition of  $\underline{B}_0$  and Europa's induced field (Figure 2(b)). The four setups including a dawn-dusk asymmetry in the atmosphere (#1–#3 and #6) largely reproduce the width and magnitude of the observed  $B_Y$  signature (Figure 2). These runs predict a broad enhancement  $\delta B_Y > 0$  in the outbound segment, centered around the isolated  $B_Y > 0$  spike seen by Juno at 09:37 UTC. The magnitude of the modeled feature matches the peak value of the observed signature ( $B_Y \approx -57 \text{ nT}$ ), while its width is overestimated. Therefore, it remains elusive whether this spike is related to Europa's plasma interaction or is magnetospheric in origin. The time series from runs #4 and #5 overestimate the strength and, especially, the width of the observed perturbations  $\delta B_Y$ . Particularly in the outbound region, an atmosphere with high column

303 densities generates  $\delta B_Y > 0$  signatures that are still discernible around 09:40 UTC, while  
 304 the observed  $B_Y$  already returns to the Jovian background field at 09:37 UTC. This again  
 305 suggests that, during the Juno flyby, the "strength" of Europa's plasma interaction (e.g.,  
 306 Simon et al. (2021)) in the sub-Jovian hemisphere may have been locally weakened.

307 The observed  $B_Z$  component reveals a broad depletion feature (i.e.,  $\delta B_Z > 0$ ) around  
 308 closest approach, commencing at 09:34 UTC. Such a depression region has already been  
 309 identified in earlier studies of Europa's interaction (e.g., Arnold, Liuzzo, and Simon (2020)):  
 310 the elevated plasma pressure associated with pick-up ions partially pushes the magne-  
 311 toospheric field lines out of the tail region. Analogous to  $B_Y$ , the width and magnitude  
 312 of the  $B_Z$  feature can be reproduced *only* by runs that include a dawn-dusk asymme-  
 313 try of Europa's neutral envelope. None of our modeled time series reproduce the double-  
 314 spike signature observed in  $B_Z$  shortly before closest approach. This may indicate that  
 315 the representation of the ionosphere in AIKEF does not include sufficient complexity to  
 316 reproduce such fine structures.

317 To provide some context for the qualitative differences in the modeled  $B_X$  signa-  
 318 tures, Figure 3 displays two-dimensional profiles of this component in the three planes  
 319 of the EPhiO system. The left column illustrates results from setup #2 (which does not  
 320 produce a  $\delta B_X < 0$  segment after Juno's closest approach), while the right column shows  
 321 output from run #4 (which suggests  $\delta B_X < 0$  in the outbound region). As can be seen  
 322 from the top and middle rows, Europa's Alfvén wings are rotated toward Jupiter around  
 323 the  $Z$  axis and northward around the  $Y$  axis. The bottom row in Figure 3 reveals the  
 324 reason for the morphological differences in  $B_X$  along the Juno trajectory. In run #2, the  
 325 core of the northern Alfvén wing ( $\delta B_X < 0$ , blue) is shifted slightly toward the  $Y <$   
 326 0 half space where the atmospheric density is larger. This happens despite the inclusion  
 327 of a small upstream flow component *toward* Jupiter. The "ray" of  $\delta B_X > 0$  in the north-  
 328 ern, Jupiter-facing half space (red in panel 3(e)) corresponds to the outer region of the  
 329  $\underline{Z}_-$  wing: in planes perpendicular to  $\underline{Z}_\pm$ , the magnetic perturbations associated with  
 330 an Alfvén wing can be represented by a two-dimensional dipole (Neubauer, 1980); i.e.,  
 331 the field lines need to *close* outside of the core region. Therefore, the field lines inside  
 332 the northern wing tube are draped ( $\delta B_X < 0$ ), but in the periphery of the wing they  
 333 appear "anti-draped" ( $\delta B_X > 0$ ).

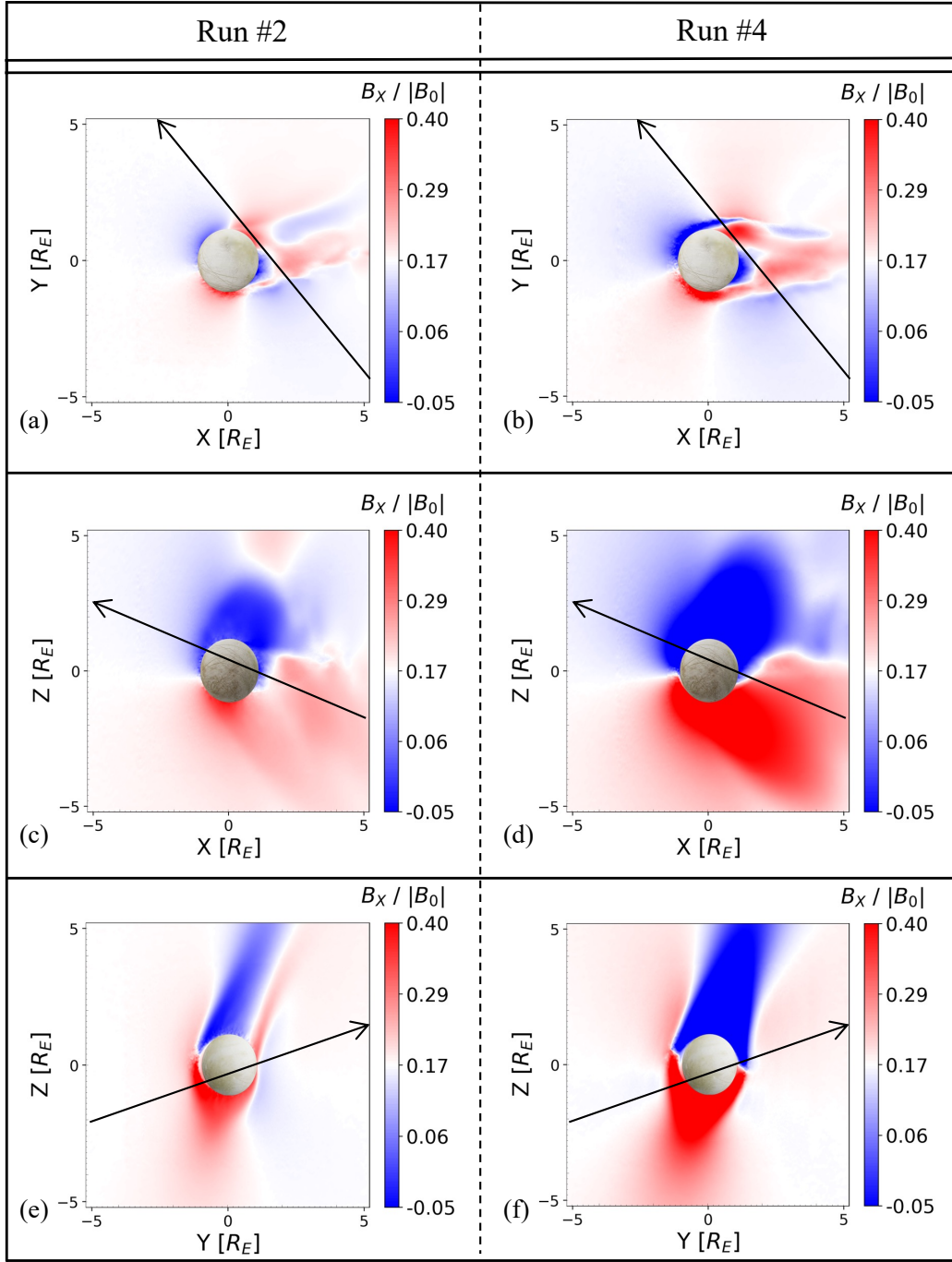


**Figure 3.** Modeled  $B_X$  components in the  $Z = 0$  (panels (a) and (b)),  $Y = 0$  (panels (c) and (d)), and  $X = 0$  planes (panels (e) and (f)). Results from setup #2 are displayed in the left column, whereas the right column shows output from run #4. In all panels, white coloring corresponds to the  $B_{0,X}$  component of the magnetospheric background field. The projection of Juno's trajectory onto each cutting plane is indicated by the black line.

334 In setup #2, the "thinning" of the northern wing tube for  $Y > 0$  caused Juno to  
 335 first travel through the center of the southern wing tube (where the field is draped,  $\delta B_X >$   
 336 0), and then graze the outer regions of the northern wing where the field is "anti-draped".  
 337 For this reason, the observed  $\delta B_X$  in the north has the *same* sign as in the south. In setup  
 338 #4, the northern wing tube (characterized by  $\delta B_X < 0$ , blue) extends slightly farther  
 339 toward Jupiter than in setup #2 (panels 3(f) versus (e)). Therefore, in run #4 Juno would  
 340 have encountered the center of the northern wing as it traveled through the  $Z > 0$  half  
 341 space. However, this picture is incompatible with observations.

## 342 4 Concluding Remarks

343 Results from the AIKEF model suggest that reproducing the large-scale shape and  
 344 magnitude of the magnetic perturbations observed during Juno's Europa flyby requires  
 345 the inclusion of a dawn-dusk asymmetry in the moon's neutral envelope. Within our model,  
 346 neither a spherically symmetric atmosphere nor the notion of a ram-wake asymmetry  
 347 can reproduce the overall shape and strength of the signatures seen by Juno. However,  
 348 this interpretation of the magnetic perturbations is possibly not unique, as we have ex-  
 349 plored only a small corner of the parameter space spanned by the upstream flow param-  
 350 eters and the neutral density profile. Various fine structures in the observed magnetic  
 351 field are not reproduced by any of the analyzed model setups. In addition, Juno was still  
 352 several  $R_E$  downstream when traveling through Europa's anti-Jovian hemisphere; i.e.,  
 353 a potential atmospheric bulge around dusk was not directly sampled. Magnetometer and  
 354 particle data from additional close flybys in Europa's dusk and dawn hemispheres are  
 355 needed to further substantiate the presence of such an atmospheric asymmetry.

356 The minimum atmospheric density at the sub-Jovian apex used in our model is by  
 357 orders of magnitude lower than proposed by Oza et al. (2019). However, the concentra-  
 358 tion of surface sputtering around Europa's dayside apex assumed by these authors is in-  
 359 consistent with more recent results that take into account the deflection of impinging mag-  
 360 netospheric particles by the draped fields (Addison et al., 2022; Addison, Liuzzo, & Si-  
 361 mon, 2023). Therefore, future search for dawn-dusk asymmetries in Europa's atmosphere  
 362 will need to combine the approach of Oza et al. (2019)—including the moon's rotation  
 363 when calculating atmospheric dynamics—with a more accurate distribution of magne-  
 364 toospheric ion and electron sputtering across the surface.

365 **Open Research Section**

366 Output from the AIKEF model and Juno magnetometer data used for compari-  
 367 son have been archived by Addison, Haynes, et al. (2023). Juno magnetometer data are  
 368 publicly available at the NASA Planetary Data System (Connerney, 2022).

369 **Acknowledgments**

370 The authors acknowledge financial support through NASA's *Solar System Workings* pro-  
 371 gram, grant # 80NSSC23K0351.

372 **References**

- 373 Addison, P., Haynes, C. M., Stahl, A., Liuzzo, L., & Simon, S. (2023). Data for  
 374 "Magnetic Signatures of the Interaction Between Europa and Jupiter's Magne-  
 375 tosphere during Juno's Close Flyby" by Addison et al., 2023 [Data set]. *Zen-*  
 376 *odo*, <https://doi.org/10.5281/zenodo.8411734>. doi: 10.5281/zenodo.8411734
- 377 Addison, P., Liuzzo, L., Arnold, H., & Simon, S. (2021). Influence of Eu-  
 378 ropa's Time-Varying Electromagnetic Environment on Magnetospheric  
 379 Ion Precipitation and Surface Weathering. *Journal of Geophysical Re-*  
 380 *search: Space Physics*, 126(5), e2020JA029087. Retrieved from <https://agupubs.onlinelibrary.wiley.com/doi/abs/10.1029/2020JA029087>  
 381 (e2020JA029087 2020JA029087) doi: <https://doi.org/10.1029/2020JA029087>
- 382 Addison, P., Liuzzo, L., & Simon, S. (2022). Effect of the Magnetospheric Plasma  
 383 Interaction and Solar Illumination on Ion Sputtering of Europa's Surface Ice.  
 384 *Journal of Geophysical Research: Space Physics*, 127(2), e2021JA030136.  
 385 Retrieved from <https://agupubs.onlinelibrary.wiley.com/doi/abs/10.1029/2021JA030136> (e2021JA030136 2021JA030136) doi: <https://doi.org/10.1029/2021JA030136>
- 386 Addison, P., Liuzzo, L., & Simon, S. (2023). Surface-Plasma Interactions at  
 387 Europa in Draped Magnetospheric Fields: The Contribution of Energetic  
 388 Electrons to Energy Deposition and Sputtering. *Journal of Geophysical Re-*  
 389 *search: Space Physics*, 128(8), e2023JA031734. Retrieved from <https://agupubs.onlinelibrary.wiley.com/doi/abs/10.1029/2023JA031734>  
 390 (e2023JA031734 2023JA031734) doi: <https://doi.org/10.1029/2023JA031734>
- 391 Arnold, H., Liuzzo, L., & Simon, S. (2019). Magnetic Signatures of a Plume at Eu-

- 396      ropa during the Galileo E26 Flyby. *Geophysical Research Letters*, 46(3), 1149–  
397      1157. doi: 10.1029/2018GL081544

398      Arnold, H., Liuzzo, L., & Simon, S. (2020). Plasma Interaction Signatures  
399      of Plumes at Europa. *Journal of Geophysical Research: Space Physics*,  
400      125(1), e2019JA027346. Retrieved from <https://agupubs.onlinelibrary.wiley.com/doi/abs/10.1029/2019JA027346> (e2019JA027346  
401      10.1029/2019JA027346) doi: 10.1029/2019JA027346

402      Arnold, H., Simon, S., & Liuzzo, L. (2020). Applying Ion Energy Spectro-  
403      grams to Search for Plumes at Europa. *Journal of Geophysical Research: Space  
404      Physics*, n/a(n/a), e2020JA028376. Retrieved from <https://agupubs.onlinelibrary.wiley.com/doi/abs/10.1029/2020JA028376> (e2020JA028376 2020JA028376) doi: 10.1029/2020JA028376

405      Baggenal, F., & Delamere, P. A. (2011). Flow of mass and energy in the magne-  
406      tospheres of Jupiter and Saturn. *Journal of Geophysical Research (Space  
407      Physics)*, 116(A5), A05209. doi: 10.1029/2010JA016294

408      Baggenal, F., & Dols, V. (2020, May). The Space Environment of Io and Eu-  
409      ropa. *Journal of Geophysical Research (Space Physics)*, 125(5), e27485. doi:  
410      10.1029/2019JA027485

411      Baggenal, F., Wilson, R. J., Siler, S., Paterson, W. R., & Kurth, W. S. (2016, May).  
412      Survey of Galileo plasma observations in Jupiter’s plasma sheet. *Journal of  
413      Geophysical Research (Planets)*, 121(5), 871-894. doi: 10.1002/2016JE005009

414      Blöcker, A., Saur, J., & Roth, L. (2016). Europa’s plasma interaction with an in-  
415      homogeneous atmosphere: Development of Alfvén winglets within the Alfvén  
416      wings. *Journal of Geophysical Research: Space Physics*, 121(10), 9794-9828.  
417      Retrieved from <https://agupubs.onlinelibrary.wiley.com/doi/abs/10.1002/2016JA022479> doi: 10.1002/2016JA022479

418      Breer, B. R., Liuzzo, L., Arnold, H., Andersson, P. N., & Simon, S. (2019). En-  
419      ergetic Ion Dynamics in the Perturbed Electromagnetic Fields Near Europa.  
420      *Journal of Geophysical Research: Space Physics*, 124(9), 7592-7613. Retrieved  
421      from <https://agupubs.onlinelibrary.wiley.com/doi/abs/10.1029/2019JA027147> doi: <https://doi.org/10.1029/2019JA027147>

422      Cassidy, T., Paranicas, C., Shirley, J., Dalton III, J., Teolis, B., Johnson, R., ...  
423      Hendrix, A. (2013). Magnetospheric ion sputtering and water ice grain size at

- 429 Europa. *Planetary and Space Science*, 77, 64 - 73. Retrieved from <http://www.sciencedirect.com/science/article/pii/S0032063312002024> (Sur-  
 430 faces, atmospheres and magnetospheres of the outer planets and their satellites  
 431 and ring systems: Part VIII) doi: <https://doi.org/10.1016/j.pss.2012.07.008>
- 432 Cervantes, S., & Saur, J. (2022, September). Constraining Europa's Subsolar At-  
 433 mosphere With a Joint Analysis of HST Spectral Images and Galileo Magnetic  
 434 Field Data. *Journal of Geophysical Research (Space Physics)*, 127(9), e30472.  
 435 doi: [10.1002/jgra.v127.9](https://doi.org/10.1002/jgra.v127.9)
- 436 Connerney, J. E. P. (2022). Juno MAG CALIBRATED DATA J V1.0,  
 437 JNO-J-3-FGM-CAL-V1.0 [Data set]. *NASA Planetary Data System*,  
 438 <https://doi.org/10.17189/1519711>. doi: [10.17189/1519711](https://doi.org/10.17189/1519711)
- 439 Connerney, J. E. P., Benn, M., Bjarno, J. B., Denver, T., Espley, J., Jorgensen,  
 440 J. L., ... Smith, E. J. (2017, November). The Juno Magnetic Field In-  
 441 vestigation. *Space Science Reviews*, 213(1-4), 39-138. doi: [10.1007/s11214-017-0334-z](https://doi.org/10.1007/s11214-017-0334-z)
- 442 Harris, C. D. K., Jia, X., & Slavin, J. A. (2022). Multi-Fluid MHD Simulations  
 443 of Europa's Plasma Interaction: Effects of Variation in Europa's Atmosphere.  
 444 *Journal of Geophysical Research: Space Physics*, 127(9), e2022JA030569.  
 445 Retrieved from <https://agupubs.onlinelibrary.wiley.com/doi/abs/10.1029/2022JA030569> (e2022JA030569 2022JA030569) doi: <https://doi.org/10.1029/2022JA030569>
- 446 Harris, C. D. K., Jia, X., Slavin, J. A., Toth, G., Huang, Z., & Rubin, M.  
 447 (2021). Multi-Fluid MHD Simulations of Europa's Plasma Interaction  
 448 Under Different Magnetospheric Conditions. *Journal of Geophysical Re-  
 449 search: Space Physics*, 126(5), e2020JA028888. Retrieved from <https://agupubs.onlinelibrary.wiley.com/doi/abs/10.1029/2020JA028888>  
 (e2020JA028888 2020JA028888) doi: <https://doi.org/10.1029/2020JA028888>
- 450 Haynes, C. M., Tippens, T., Addison, P., Liuzzo, L., Poppe, A. R., & Simon, S.  
 451 (2023). Emission of Energetic Neutral Atoms from the Magnetosphere-  
 452 Atmosphere Interactions at Callisto and Europa. *Journal of Geophysical Re-  
 453 search: Space Physics*, 128(10), e2023JA031931. doi: [10.1029/2023JA031931](https://doi.org/10.1029/2023JA031931)
- 454 Jia, X., Kivelson, M. G., Khurana, K. K., & Kurth, W. S. (2018). Evidence of a  
 455 plume on Europa from Galileo magnetic and plasma wave signatures. *Nature*

- 462 *Astronomy*, 2(6), 459–464. Retrieved from <https://doi.org/10.1038/s41550-018-0450-z>

463 Kivelson, M. G., Bagenal, F., Kurth, W. S., Neubauer, F. M., Paranicas, C., &

464 Saur, J. (2004). Magnetospheric interactions with satellites. In F. Bagenal,

465 T.E. Dowling and W.B. McKinnon (Ed.), *Jupiter. The planet, satellites and*

466 *magnetosphere* (pp. 513–536). Cambridge Univ. Press.

467

468 Kivelson, M. G., Khurana, K. K., Russell, C. T., Volwerk, M., Walker, R. J., & Zim-

469 mer, C. (2000). Galileo Magnetometer Measurements: A Stronger Case for

470 a Subsurface Ocean at Europa. *Science*, 289(5483), 1340–1343. Retrieved

471 from <https://science.sciencemag.org/content/289/5483/1340> doi:

472 10.1126/science.289.5483.1340

473 Kivelson, M. G., Khurana, K. K., & Volwerk, M. (2009). Europa’s Interaction

474 with the Jovian Magnetosphere. In R. T. Pappalardo, W. B. McKinnon, &

475 K. K. Khurana (Eds.), *Europa* (p. 545).

476 Liuzzo, L., Feyerabend, M., Simon, S., & Motschmann, U. (2015). The impact

477 of Callisto’s atmosphere on its plasma interaction with the Jovian magneto-

478 sphere. *Journal of Geophysical Research: Space Physics*, 120(11), 9401–9427.

479 Retrieved from <https://agupubs.onlinelibrary.wiley.com/doi/abs/10.1002/2015JA021792> doi: 10.1002/2015JA021792

480 Müller, J., Simon, S., Motschmann, U., Schüle, J., Glassmeier, K., & Pringle,

481 G. J. (2011). A.I.K.E.F.: Adaptive hybrid model for space plasma sim-

482 ulations. *Computer Physics Communications*, 182(4), 946–966, doi:

483 10.1016/j.cpc.2010.12.033.

484 Neubauer, F. M. (1980). Nonlinear standing Alfvén wave current system at Io - The-

485 ory. *J. Geophys. Res.*, 85, 1171–1178. doi: 10.1029/JA085iA03p01171

486

487 Neubauer, F. M. (1998). The sub-Alfvénic interaction of the Galilean satellites with

488 the Jovian magnetosphere. *J. Geophys. Res.*, 103, 19843–19866. doi: 10.1029/97JE03370

489

490 Neubauer, F. M. (1999). Alfvén wings and electromagnetic induction in the inte-

491 riors: Europa and Callisto. *Journal of Geophysical Research (Space Physics)*,

492 104(A12), 28671–28684. doi: 10.1029/1999JA900217

493 Oza, A. V., Leblanc, F., Johnson, R. E., Schmidt, C., Leclercq, L., Cassidy, T. A.,

494 & Chaufray, J.-Y. (2019, March). Dusk over dawn O<sub>2</sub> asymmetry in Eu-

- ropo's near-surface atmosphere. *Planetary and Space Science*, 167, 23-32. doi: 10.1016/j.pss.2019.01.006

Plainaki, C., Cassidy, T. A., Shematovich, V. I., Milillo, A., Wurz, P., Vorburger, A., ... Teolis, B. (2018, February). Towards a Global Unified Model of Europa's Tenuous Atmosphere. *Space Science Reviews*, 214(1), 40. doi: 10.1007/s11214-018-0469-6

Roth, L. (2021). A Stable H<sub>2</sub>O Atmosphere on Europa's Trailing Hemisphere From HST Images. *Geophysical Research Letters*, 48(20), e2021GL094289. Retrieved from <https://agupubs.onlinelibrary.wiley.com/doi/abs/10.1029/2021GL094289> (e2021GL094289 2021GL094289) doi: <https://doi.org/10.1029/2021GL094289>

Roth, L., Rutherford, K. D., Saur, J., Strobel, D. F., Feldman, P. D., McGrath, M. A., & Nimmo, F. (2014). Orbital apocenter is not a sufficient condition for HST/STIS detection of Europa's water vapor aurora. *Proceedings of the National Academy of Sciences*, 111(48), E5123–E5132. Retrieved from <https://www.pnas.org/content/111/48/E5123> doi: 10.1073/pnas.1416671111

Rubin, M., Jia, X., Altweig, K., Combi, M. R., Daldorff, L. K. S., Gombosi, T. I., ... Wurz, P. (2015). Self-consistent multifluid MHD simulations of Europa's exospheric interaction with Jupiter's magnetosphere. *Journal of Geophysical Research: Space Physics*, 120(5), 3503-3524. Retrieved from <https://agupubs.onlinelibrary.wiley.com/doi/abs/10.1002/2015JA021149> doi: 10.1002/2015JA021149

Saur, J., Strobel, D. F., & Neubauer, F. M. (1998). Interaction of the Jovian magnetosphere with Europa: Constraints on the neutral atmosphere. *Journal of Geophysical Research: Planets*, 103(E9), 19947-19962. Retrieved from <https://agupubs.onlinelibrary.wiley.com/doi/abs/10.1029/97JE03556> doi: 10.1029/97JE03556

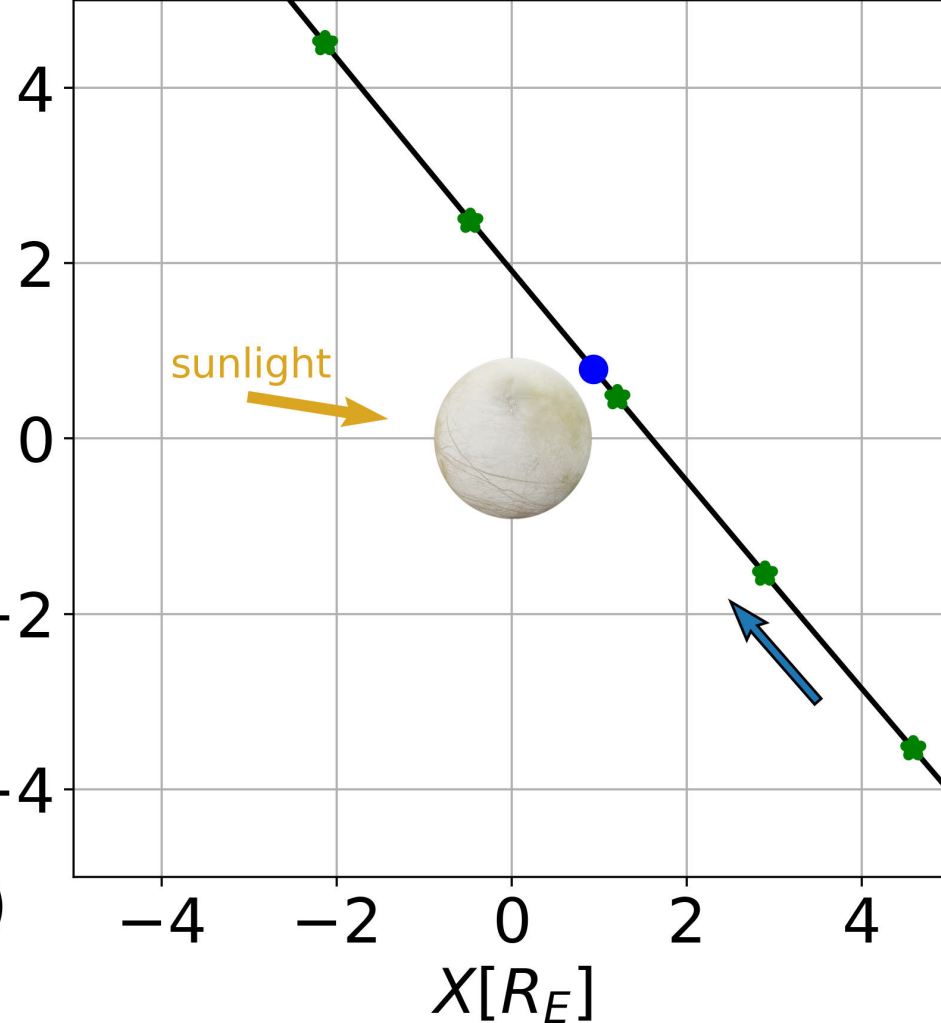
Schilling, N., Neubauer, F. M., & Saur, J. (2007). Time-varying interaction of Europa with the jovian magnetosphere: Constraints on the conductivity of Europa's subsurface ocean. *Icarus*, 192(1), 41 - 55. Retrieved from <http://www.sciencedirect.com/science/article/pii/S0019103507002837> doi: <https://doi.org/10.1016/j.icarus.2007.06.024>

- 528 Simon, S., Liuzzo, L., & Addison, P. (2021). Role of the ionospheric conductance  
529 profile in sub-alfvénic moon-magnetosphere interactions: An analytical model.  
530 *Journal of Geophysical Research: Space Physics*, 126(7), e2021JA029191.  
531 Retrieved from <https://agupubs.onlinelibrary.wiley.com/doi/abs/10.1029/2021JA029191> (e2021JA029191 2021JA029191) doi: <https://doi.org/10.1029/2021JA029191>
- 534 Simon, S., & Motschmann, U. (2009). Titan's induced magnetosphere under non-  
535 ideal upstream conditions: 3D multi-species hybrid simulations. *Planet. Space  
536 Sci.*, 57(14–15), 2001–2015, doi: 10.1016/j.pss.2009.08.010.
- 537 Volwerk, M., Khurana, K., & Kivelson, M. (2007, 05). Europa's Alfvén wing:  
538 Shrinkage and displacement influenced by an induced magnetic field. *Annales  
539 Geophysicae*, 25. doi: 10.5194/angeo-25-905-2007
- 540 Zimmer, C., Khurana, K. K., & Kivelson, M. G. (2000). Subsurface Oceans on  
541 Europa and Callisto: Constraints from Galileo Magnetometer Observations.  
542 *Icarus*, 147(2), 329–347. doi: 10.1006/icar.2000.6456

**Figure 1.**

$Y[R_E]$ 

(a)

 $Z[R_E]$ 

(b)

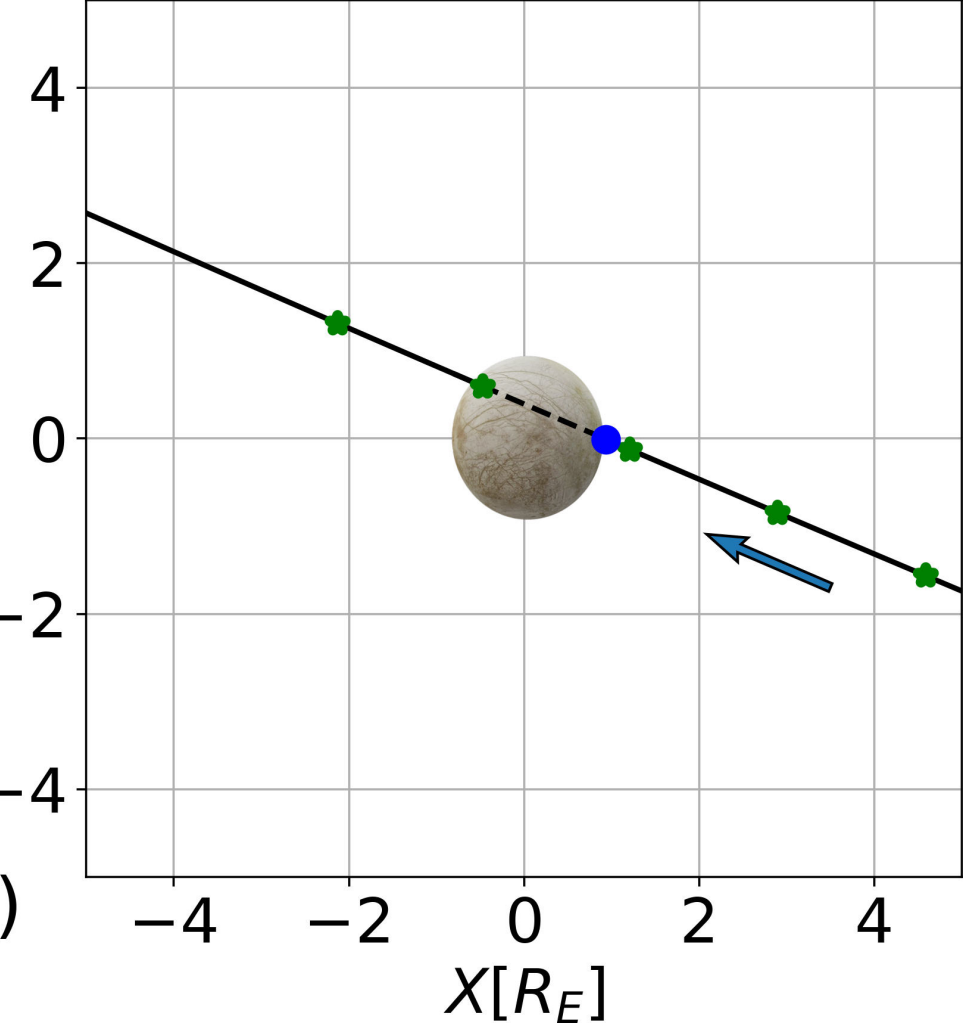
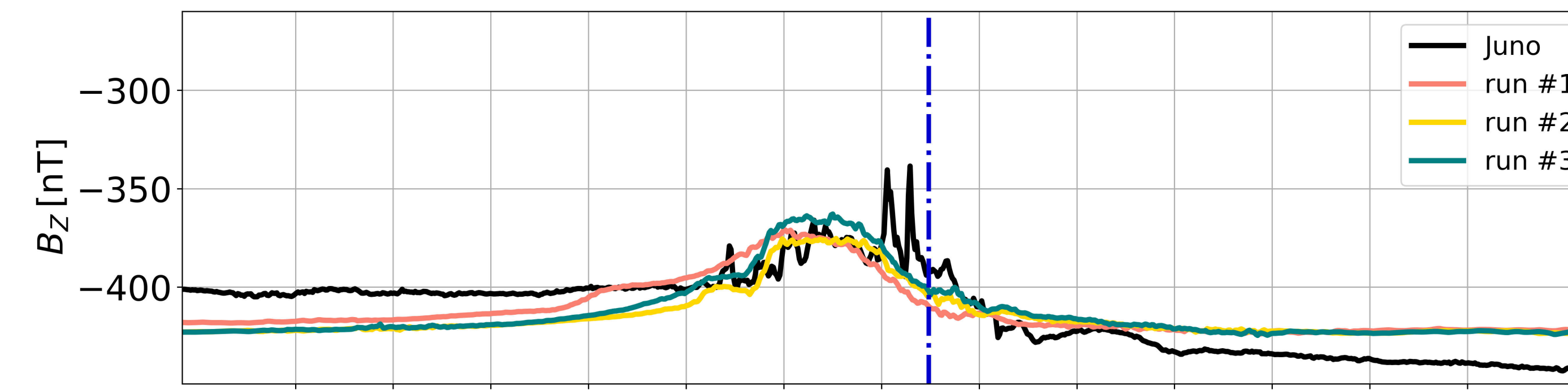
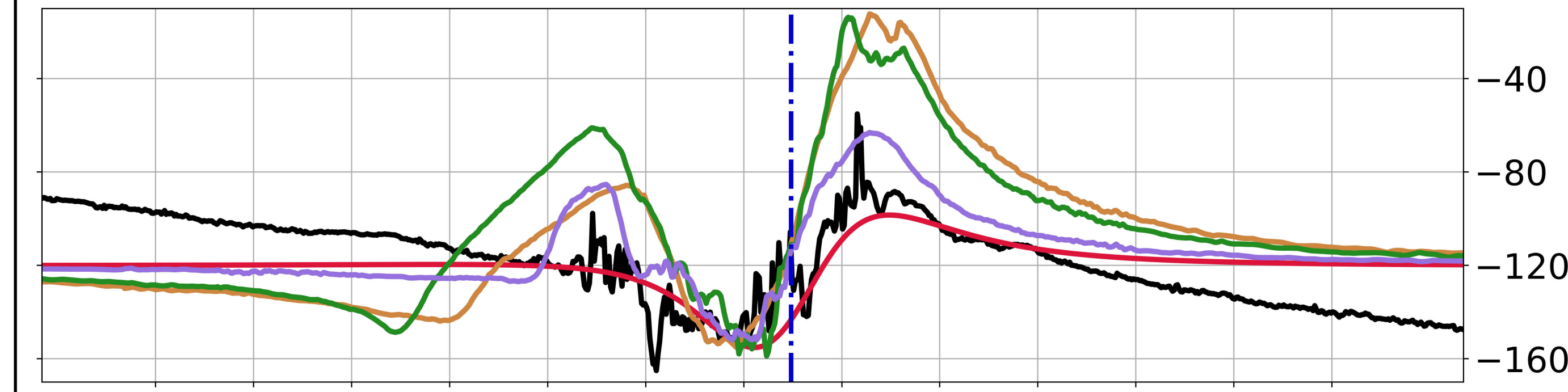
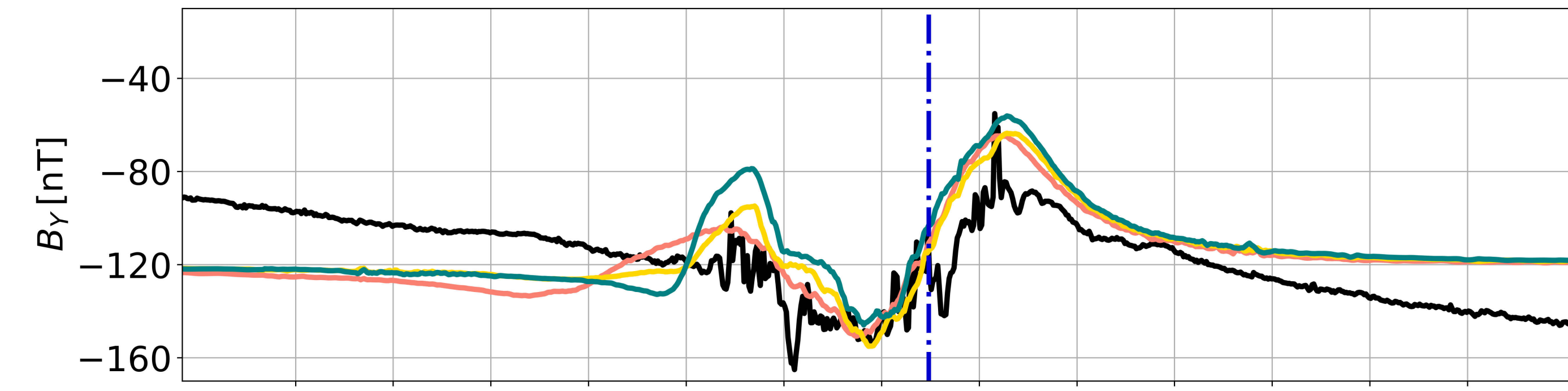
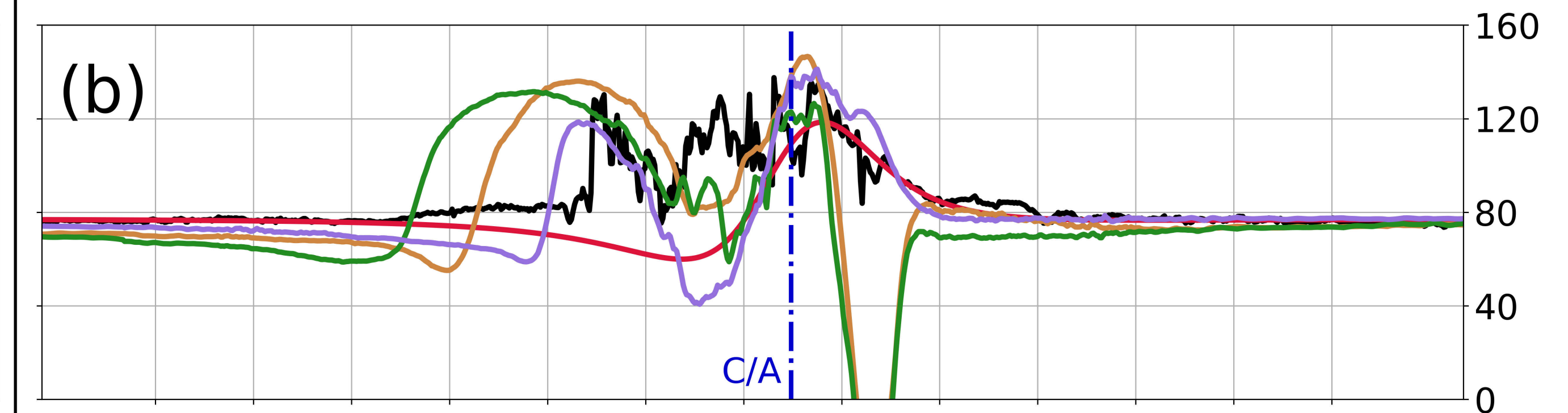
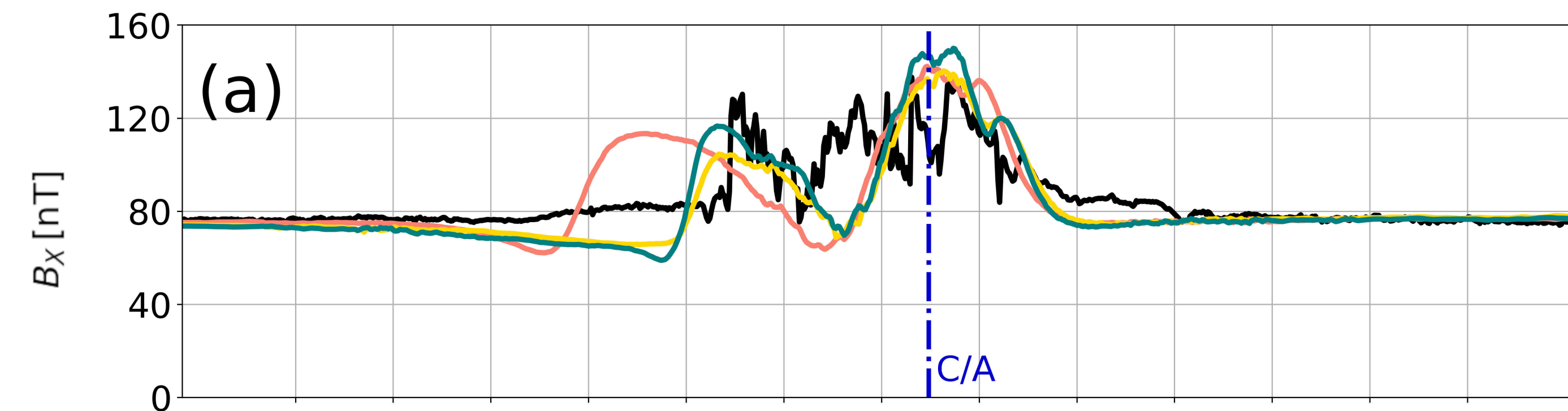
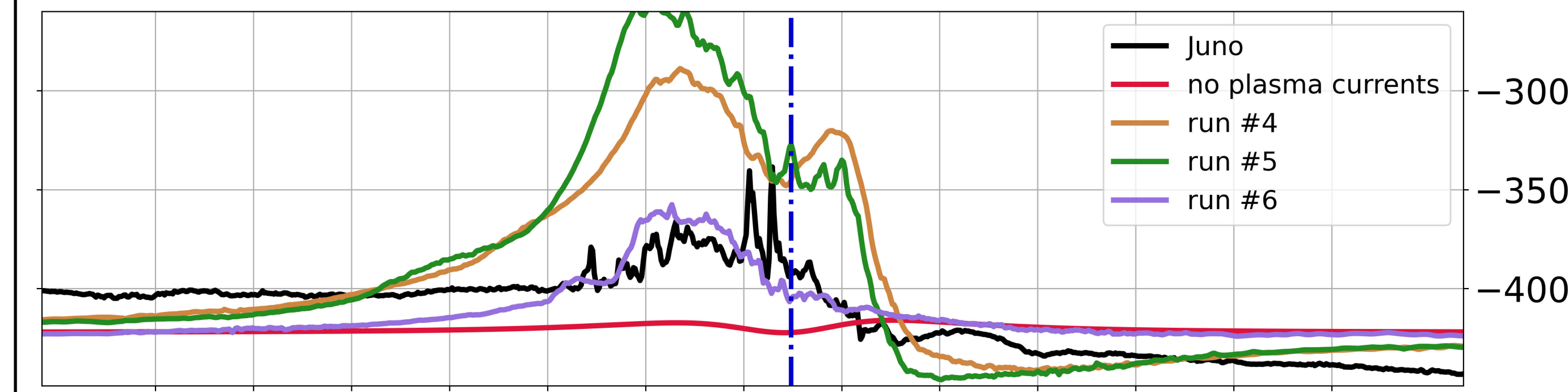


**Figure 2.**



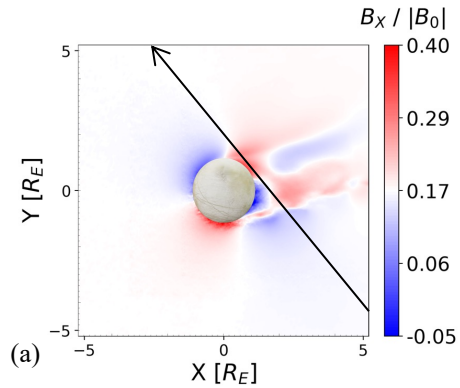
time [UTC]	09:30	09:33	09:36	09:39	09:42
$X[R_E]$	4.58	2.89	1.21	-0.47	-2.13
$Y[R_E]$	-3.54	-1.54	0.47	2.49	4.51
$Z[R_E]$	-1.56	-0.84	-0.12	0.60	1.32
$r[R_E]$	5.99	3.38	1.30	2.60	5.16



time [UTC]	09:30	09:33	09:36	09:39	09:42
$X[R_E]$	4.58	2.89	1.21	-0.47	-2.13
$Y[R_E]$	-3.54	-1.54	0.47	2.49	4.51
$Z[R_E]$	-1.56	-0.84	-0.12	0.60	1.32
$r[R_E]$	5.99	3.38	1.30	2.60	5.16

**Figure 3.**

Run #2



Run #4

